

# Fourier Spectral Methods for Degasperis–Procesi Equation with Discontinuous Solutions

Yinhua Xia

Received: 3 October 2013 / Revised: 9 February 2014 / Accepted: 3 March 2014 /  
Published online: 15 March 2014  
© Springer Science+Business Media New York 2014

**Abstract** In this paper, we develop, analyze and test the Fourier spectral methods for solving the Degasperis–Procesi (DP) equation which contains nonlinear high order derivatives, and possibly discontinuous or sharp transition solutions. The  $L^2$  stability is obtained for general numerical solutions of the Fourier Galerkin method and Fourier collocation (pseudospectral) method. By applying the Gegenbauer reconstruction technique as a post-processing method to the Fourier spectral solution, we reduce the oscillations arising from the discontinuity successfully. The numerical simulation results for different types of solutions of the nonlinear DP equation are provided to illustrate the accuracy and capability of the methods.

**Keywords** Degasperis–Procesi equation · Discontinuous solution · Fourier Galerkin method · Fourier collocation method ·  $L^2$  stability · Gegenbauer reconstruction

## 1 Introduction

In this paper, we consider the Fourier spectral approximation to the Degasperis–Procesi(DP) equation

$$u_t - u_{txx} + 4f(u)_x = f(u)_{xxx}, \quad (1)$$

for a real function  $u(x, t)$  of the two variables  $x$  and  $t$ , where  $f(u) = u^2/2$ . DP equation is a real nonlinear partial differential equation (PDE) which models propagation of nonlinear dispersive waves and is solvable by the methods of soliton theory. The DP equation is very special because it belongs to the class of integrable equations, that is PDEs with infinitely many conservation laws. Based on multiscale perturbation theory, Degasperis and

---

Research supported by NSFC Grant No.11101400, No.11371342, Doctoral Fund of Ministry of Education of China No. 20113402120015 and SRF for ROCS SEM.

---

Y. Xia (✉)  
School of Mathematical Sciences, University of Science and Technology of China,  
Hefei 230026, Anhui, P.R. China  
e-mail: yhxia@ustc.edu.cn

Procesi [12] found there are only three PDEs, which satisfy the integrability conditions, of the following family

$$u_t + cu_x + \kappa u_{xxx} - \epsilon^2 u_{ixx} - \epsilon^2 d(uu_{xxx} + bu_x u_{xx}) + auu_x = 0, \tag{2}$$

namely, the Korteweg de Vries (KdV) equation for  $\epsilon = 0$ , the Camassa–Holm (CH) equation for  $b = 2$  and  $a = 3d$ , and the DP equation for  $b = 3$  and  $a = 4d$ . This is how the DP equation has been first found while the other two equations, i.e. the KdV and CH equations, were already known to be integrable by different arguments. The DP equation is covariant under the group of transformations  $u(x, t) \rightarrow u'(x, t) = \alpha u(\beta x + \gamma t, t) + \delta$ , and by a suitable choice of the parameters  $\alpha, \beta, \gamma, \delta$ , the coefficients can be fixed as  $\epsilon = 1, c = 0, \kappa = 0$  and  $d = 1$ . With this choice of the coefficients (after dropping the prime) the DP equation takes the neat form of the Eq. (1). This PDE is not only of mathematical interest but it has also proved to be an approximate model of shallow water wave propagation in the small amplitude and long wavelength regime [11, 14, 24, 25]. Indeed, in this approximation, waves are assumed to propagate in one direction over a flat bottom with no viscosity, no shear stress and no compressibility under the influence of gravity and surface tension. The dependent variable  $u$  is the horizontal velocity field while the independent variables  $x$  and  $t$  are the space and time coordinates. The coefficients in (2) have physical meaning, where  $c$  is the linear wave velocity, the coefficients  $\epsilon$  and  $\kappa$  are related to linear dispersion and  $d$  comes from the Euler equation of motion.

The well-known KdV equation describes the unidirectional propagation of waves at free surface of shallow water under the influence of the gravity. The solitary waves of the KdV equation are solitons. The CH equation models the unidirectional propagation of shallow water waves over a flat bottom or the propagation of axially symmetric waves in hyperelastic rods. The advantage of the CH equation in comparison with the KdV equation lies in that the CH equation has the peaked solitary wave (peakon) solutions [3], which have the jumps in its first order derivative, for example  $u(x, t) = ce^{-|x-ct|}$ . Despite the similarities to the CH equation, the DP equation is truly different from the CH equation. The DP equation has not only peakon solutions [13], but also shock waves [8, 28], for example  $u(x, t) = -\frac{1}{t+c} \text{sign}(x)e^{-|x|}, c > 0$ . Also, the Lax pairs of the CH and DP equations are different. Although the bi-Hamiltonian structures of the CH and DP equations provide an infinite number of conservation laws, the conservation laws of DP equation are much weaker than those of the CH equation. The first three conservation laws of the DP equation are

$$E_1 = \int (u - u_{xx})dx, \quad E_2 = \int (u - u_{xx})vdx; \quad E_3 = \int u^3 dx,$$

where  $4v - v_{xx} = u$ . And the corresponding conservation laws of the CH equation are

$$H_1 = \int (u - u_{xx})dx, \quad H_2 = \int (u^2 + u_x^2)dx; \quad H_3 = \int (u^3 + uu_x^2)dx.$$

The conservation law  $H_2$  plays an important role in the analysis and development of numerical schemes of the CH equation. But the conservation laws of the DP equation can not control the  $H^1$  norm. Meanwhile, the lack of smoothness of the solution make it challenging to design stable and high order accurate numerical schemes for the DP equation. Coclite and Karlsen proved existence and uniqueness results for entropy weak solutions belonging to the class  $L^1 \cap BV$  in [8] and uniqueness result for entropy weak solutions by replacing the Kružkov-type entropy inequalities by an Oleinik-type estimate in [9]. Coclite, Karlsen and Risebro [10] constructed several operator splitting schemes and proved that solutions of these finite difference schemes converge to entropy weak solutions. Moreover, they provided several

numerical examples to show that shock solutions can form independently of the smoothness of the initial data. Another operator splitting method was proposed for the DP equation in [15], which is based on the second-order TVD scheme and linearized implicit finite difference method. Miyatake and Matsuo [29] proposed two conservative finite difference schemes to preserve two invariants  $E_2$  and  $E_3$  for the DP equation. And compact finite difference scheme has been used by Yu et al. [34] with symplectic implicit Runge-Kutta time integration. In [23], a particle method based on the multi-shock peakon solutions was investigated for entropy weak solutions of the DP equation numerically. Local discontinuous Galerkin (LDG) and direct DG finite element methods have been designed for the DP equation by Xu and Shu [33] and Liu et al. [27], after developing the LDG methods for the CH equation [32].

The application of spectral methods for the solution of partial differential equation (PDE) has traditionally been centered around problems with a certain amount of inherent regularity of the solutions. When the solution of nonlinear PDE admits discontinuity, e.g., hyperbolic conservation laws, the nonlinear mixing of Gibbs oscillations with approximate solution will eventually cause the scheme to become unstable. Moreover, even if stability is maintained, the computed solution appears only first-order accurate. However, many significant advances have been made to establish the soundness of the spectral approach for such problem in last decades, see Bernardi et al. [1], Boyd [2], Canuto et al. [4–6], Gottlieb and Orszag [19], Guo [21], Hesthaven et al. [22], Karniadakis et al. [26], Shen et al. [30], and the reference therein. It is confirmed that the superior behavior of these methods for smooth problems carries over to problems involving nonsmooth solutions.

The remains of this paper is organized as follows. In Sect. 2 we develop the Fourier Galerkin and collocation spectral methods for the DP equation. The  $L^2$  stability has also been proved for both methods. The exponential filter is adopted to stable the methods when the shock is formed in the DP equation. In Sect. 3 we resolve the shock sharply through the Gegenbauer reconstruction of an exponentially convergent approximation to a piecewise smooth function using the global information at the final time step. Also the shock location is detected by using the generalized Fourier partial sum. Sect. 4 contains the numerical tests to demonstrate the accuracy and capacity of the methods. Concluding remarks are given in Sect. 5.

## 2 Fourier Spectral Method

Consider the DP Eq. (1) with the initial condition  $u(x, 0) = u_0(x)$  in the interval  $[-L, L]$ , and assume the solution satisfies the periodic boundary condition. The inner product and the associated norm of  $L^2([-L, L])$  space are denoted by

$$(u, w) := \int_{-L}^L u(x)\bar{w}(x)dx, \quad \|u\|_{L^2} = \sqrt{(u, u)}.$$

An important tool in the proof of  $L^2$  norm stability of  $u$  is the quantity  $v$ , which has appeared in the energy  $E_2$  of the DP equation. We can obtain the  $L^2$  norm bound on the solution  $u$  in terms of the initial data  $u_0$ , by noticing that the following energy stability of  $v$  has been derived in [8]

$$\frac{d}{dt} \int_{-L}^L (2v^2 + \frac{5}{2}v_x^2 + \frac{1}{2}v_{xx}^2)dx = 0. \quad (3)$$

It follows that  $u, v \in L^\infty(\mathbb{R}^+, L^2([-L, L]))$ . And then we can get the  $L^2$  stability of  $u$  that

$$\|u(x, t)\|_{L^2} \leq 2 \|u_0(x)\|_{L^2},$$

which is the key to develop numerical schemes.

By introducing the auxiliary variable  $m$ , the DP equation is equivalent to the following system of two coupled differential equations

$$\begin{cases} m_t + um_x + 3u_xm = 0, \\ u - u_{xx} = m. \end{cases} \tag{4}$$

The DP equation can also be written in the following hyperbolic-elliptic system

$$\begin{cases} u_t + f(u)_x + P_x = 0, \\ -P_{xx} + P = \frac{3}{2}u^2. \end{cases} \tag{5}$$

### 2.1 Fourier Galerkin Method

Based on these two different forms, we will develop Fourier Galerkin spectral methods for the DP equation firstly and prove the corresponding numerical solutions are also  $L^2$  stable.

In the Fourier Galerkin method, we seek the approximation solution  $u_h(x, t)$  from the space

$$B_N = \text{span}\{e^{ik\frac{\pi}{L}x}\}_{|k|\leq N},$$

i.e.  $u_N(x, t) = \sum_{|k|\leq N} a_k(t)e^{ik\frac{\pi}{L}x}$ . Note that  $a_k(t)$  are unknown coefficients which will be determined by the method. In general, the coefficients  $a_k(t)$  of the approximation are not equivalent to the Fourier expansion coefficients  $\hat{u}_k = \frac{1}{2L} \int_{-L}^L u(x, t)e^{-ik\frac{\pi}{L}x} dx$  of the exact solution  $u(x, t)$ . In the Fourier Galerkin method, the coefficients  $a_k(t)$  are determined by the

**scheme I:** Find  $u_h \in B_N$ , such that

$$\begin{cases} (\partial_t m_h + 3u_h(m_h)_x + m_h(u_h)_x, w_h) = 0, \\ (u_h - (u_h)_{xx}, q_h) = (m_h, q_h) \end{cases} \tag{6}$$

for all test function  $w_h, q_h \in B_N$ , in  $[-L, L]$ , or the **scheme II:** Find  $u_h, P_h \in B_N$ , such that

$$\begin{cases} (\partial_t u_h + (f(u_h) + P_h)_x, w_h) = 0, \\ (P_h - (P_h)_{xx}, q_h) = (3f(u_h), q_h) \end{cases} \tag{7}$$

for all test functions  $w_h, q_h \in B_N$ , in  $[-L, L]$ . It is equivalent to set the test functions  $w_h, q_h = e^{ik\frac{\pi}{L}x}$  for  $|k| \leq N$ . Then it leads to  $2N + 1$  ordinary differential equations for the coefficients  $a_k(t)$ , and the initial conditions are  $a_k(0) = \frac{1}{2L} \int_{-L}^L u_0(x)e^{-ik\frac{\pi}{L}x} dx$ .

In order to prove the  $L^2$  bound of the numerical solution  $u_h$  of two schemes, similarly we will introduce the auxiliary variable  $v_h \in B_N$  in projection form, such that

$$(4v_h - (v_h)_{xx}, w_h) = (u_h, w_h) \tag{8}$$

for all  $w_h \in B_N$ . Then we have the following energy stability relation lemma.

#### Lemma 2.1

$$\frac{d}{dt} \int_{-L}^L \left( 2v_h^2 + \frac{5}{2}(v_h)_x^2 + \frac{1}{2}(v_h)_{xx}^2 \right) dx = \int (u_h)_t (v_h - (v_h)_{xx}) dx, \tag{9}$$

*Proof* It follows by taking the time derivative of the Eq. (8) and choosing the test function  $w_h = v_h - (v_h)_{xx}$  which belongs to the space  $B_N$ .  $\square$

Using this lemma, we can prove the following energy conservation of  $v_h$  for both scheme I and II.

**Proposition 2.2** *For the Fourier Galerkin scheme I and II, the following energy of  $v_h$  is conserved*

$$\frac{d}{dt} \int_{-L}^L \left( 2v_h^2 + \frac{5}{2}(v_h)_x^2 + \frac{1}{2}(v_h)_{xx}^2 \right) dx = 0. \tag{10}$$

*Proof* In scheme I, by the integration by parts firstly and choosing the test function  $w_h = v_h$ , we have

$$(\partial_t u_h, v_h - (v_h)_{xx}) - (f(u_h), (4v_h - (v_h)_{xx})_x) = 0.$$

From the Eq. (8), we can get

$$(4v_h - (v_h)_{xx}, f(u_h)_x) = (u_h, f(u_h)_x).$$

Substituting the last equation and the Eq. (9) in the lemma 2.1, yields

$$\frac{d}{dt} \int_{-L}^L \left( 2v_h^2 + \frac{5}{2}(v_h)_x^2 + \frac{1}{2}(v_h)_{xx}^2 \right) dx - (f(u_h), (u_h)_x) = 0.$$

It shows that the quantity  $\int_{-L}^L \left( 2v_h^2 + \frac{5}{2}(v_h)_x^2 + \frac{1}{2}(v_h)_{xx}^2 \right) dx$  is conserved and the energy conservation of  $v_h$  (10) is obtained.

In scheme II, by the definition of the space  $B_N$ , we can choose the test function  $w_h = v_h - (v_h)_{xx} \in B_N$  and  $q_h = (v_h)_x \in B_N$ . Then we get

$$\begin{aligned} (\partial_t u_h + (f(u_h) + P_h)_x, v_h - (v_h)_{xx}) &= 0, \\ (P_h - (P_h)_{xx}, (v_h)_x) &= (3f(u_h), (v_h)_x). \end{aligned}$$

Summing up these two equation, we can obtain the similar conservation laws as in the scheme I

$$(\partial_t u_h, v_h - (v_h)_{xx}) + (f(u_h)_x, 4v_h - (v_h)_{xx}) = 0,$$

which implies the energy conservation of  $v_h$  of the scheme II by using the lemma 2.1.  $\square$

It follows from this proposition that the  $L^2$  norm  $u_h$  is stable for both schemes.

**Proposition 2.3** *For the Fourier Galerkin scheme I and II, the  $L^2$  norm of  $u_h$  is stable,*

$$\|u_h(\cdot, t)\|_{L^2} \leq 2 \|u_h(\cdot, 0)\|_{L^2}.$$

*Proof* Using the projection in the Eq. (8), we find

$$\begin{aligned} (u_h, u_h) &= (4v_h - (v_h)_{xx}, 4v_h - (v_h)_{xx}) \\ &= 16(v_h, v_h) + 8((v_h)_x, (v_h)_x) + ((v_h)_{xx}, (v_h)_{xx}). \end{aligned}$$

It implies the following two inequalities,

$$\begin{aligned} (u_h, u_h) &\leq 8 \left( 2(v_h, v_h) + \frac{5}{2}((v_h)_x, (v_h)_x) + \frac{1}{2}((v_h)_{xx}, (v_h)_{xx}) \right), \\ (u_h, u_h) &\geq 2 \left( 2(v_h, v_h) + \frac{5}{2}((v_h)_x, (v_h)_x) + \frac{1}{2}((v_h)_{xx}, (v_h)_{xx}) \right). \end{aligned}$$

From the energy conservation of  $v_h$  in the proposition 2.2, we can derive

$$\begin{aligned} \|u_h(\cdot, t)\|_{L^2}^2 &\leq 8 \left( 2(v_h, v_h) + \frac{5}{2}((v_h)_x, (v_h)_x) + \frac{1}{2}((v_h)_{xx}, (v_h)_{xx}) \right) (t) \\ &= 8 \left( 2(v_h, v_h) + \frac{5}{2}((v_h)_x, (v_h)_x) + \frac{1}{2}((v_h)_{xx}, (v_h)_{xx}) \right) (0) \\ &\leq 4 \|u_h(\cdot, 0)\|_{L^2}^2. \end{aligned}$$

Thus, the  $L^2$  norm stability of  $u_h$  is obtained. □

### 2.2 Fourier Collocation Method

Rather than requiring that the orthogonal projection of the DP equation onto  $B_N$  vanishes, one can require that the equation is satisfied on some set of grid points  $x_j$ . We refer to this grid as the collocation grid. And this kind of method is known as the Fourier collocation spectral method or pseudospectral method. In the following, we deal with approximation base on the grid

$$x_j = \frac{2Lj}{2N + 1}, \quad j = -N, \dots, N.$$

In the Fourier collocation method we seek solution,  $u_h \in B_N$ , of the form

$$u_h(x, t) = \sum_{|j| \leq N} u_h(x_j, t) g_j(x), \tag{11}$$

where  $g_j(x)$  is the Lagrange interpolation trigonometric polynomial for the collocation grid. Here we will introduce the notation  $I_N u(x, t)$  to represent the interpolation operator, i.e.,

$$I_N u(x, t) = \sum_{|j| \leq N} u(x_j, t) g_j(x),$$

based on the collocation grid. Note that the derivative of the interpolation is not the interpolation of the derivative, i.e.,

$$I_N(u_x) \neq (I_N u)_x,$$

unless  $u(x) \in B_N$ . But the quadrature formula is highly accurate, that

$$\frac{1}{2L} \int_{-L}^L u(x) dx = \frac{1}{2N + 1} \sum_{|j| \leq N} u(x_j) \tag{12}$$

is exact for all  $u(x) \in B_{2N}$ . Let us define the discrete inner product and  $L^2$  equivalent norm as

$$(u, w)_h = \frac{2L}{2N + 1} \sum_{|j| \leq N} u(x_j) w(x_j), \quad \|u\|_h = \sqrt{(u, u)_h}.$$

As a consequence of the exactness of the quadrature formula for trigonometric function we have

$$(u, w)_h = (u, w), \quad \|u\|_h = \|u\|_{L^2}, \quad \forall u, w \in B_N. \tag{13}$$

To obtain the similar discrete  $L^2$  stability for the Fourier collocation method as for the Fourier Galerkin method, we write down the following collocation scheme. In the Fourier collocation **scheme III**, the approximation solution  $u_h$  of the DP equation satisfies the equation

$$\begin{aligned} \frac{\partial(u_h - (u_h)_{xx})}{\partial t}(x_j, t) + 4 \left( \frac{2}{3} \frac{\partial I_N f(u_h)}{\partial x} + \frac{1}{3} I_N(u_h(u_h)_x) \right)(x_j, t) \\ - \left( \frac{2}{3} \frac{\partial I_N f(u_h)}{\partial x} + \frac{1}{3} I_N(u_h(u_h)_x) \right)_{xx}(x_j, t) = 0. \quad j = -N, \dots, N. \end{aligned} \tag{14}$$

Due to the aliasing errors and the mixing of these through the nonlinear term, the approximations  $\frac{\partial I_N f(u_h)}{\partial x}$  and  $I_N(u_h(u_h)_x)$  are not equivalent and will in general yield different results. It is the key to obtain  $L^2$  stability for the collocation method by splitting  $f(u)_x$  into  $\frac{2}{3} \frac{\partial I_N f(u_h)}{\partial x} + \frac{1}{3} I_N(u_h(u_h)_x)$  form.

Similar to the Fourier Galerkin method, we introduce the auxiliary variable  $v_h \in B_N$  in the collocation form, such that

$$(4v_h - (v_h)_{xx})(x_j, t) = u_h(x_j, t), \quad j = -N, \dots, N. \tag{15}$$

Since  $B_N$  is a finite dimensional space, this equation is exactly the same as the Eq. (8). Thus the Lemma 2.1 is also true for the collocation scheme III.

**Proposition 2.4** *For the Fourier collocation scheme III, the following energy of  $v_h$  is conserved*

$$\frac{d}{dt} \int_{-L}^L \left( 2v_h^2 + \frac{5}{2}(v_h)_x^2 + \frac{1}{2}(v_h)_{xx}^2 \right) dx = 0. \tag{16}$$

*Proof* Multiplying by  $\frac{2L}{2N+1} v_h(x_j, t)$  to the scheme III and summing over all the collocation points we obtain

$$\begin{aligned} \left( \frac{\partial(u_h - (u_h)_{xx})}{\partial t}, v_h \right)_h + \left( 4 \left( \frac{2}{3} \frac{\partial I_N f(u_h)}{\partial x} + \frac{1}{3} I_N(u_h(u_h)_x) \right), v_h \right)_h \\ - \left( \left( \frac{2}{3} \frac{\partial I_N f(u_h)}{\partial x} + \frac{1}{3} I_N(u_h(u_h)_x) \right)_{xx}, v_h \right)_h = 0. \end{aligned}$$

Observe that the term  $\frac{\partial I_N f(u_h)}{\partial x}, I_N(u_h(u_h)_x) \in B_N$ , so the quadrature rule (12) is exact. Thus,

$$\begin{aligned} \left( \left( \frac{2}{3} \frac{\partial I_N f(u_h)}{\partial x} + \frac{1}{3} I_N(u_h(u_h)_x) \right)_{xx}, v_h \right)_h &= \left( \left( \frac{2}{3} \frac{\partial I_N f(u_h)}{\partial x} + \frac{1}{3} I_N(u_h(u_h)_x) \right)_{xx}, v_h \right) \\ &= \left( \left( \frac{2}{3} \frac{\partial I_N f(u_h)}{\partial x} + \frac{1}{3} I_N(u_h(u_h)_x) \right), (v_h)_{xx} \right) \\ &= \left( \left( \frac{2}{3} \frac{\partial I_N f(u_h)}{\partial x} + \frac{1}{3} I_N(u_h(u_h)_x) \right), (v_h)_{xx} \right)_h. \end{aligned}$$

Hence

$$\left(\frac{\partial(u_h - (u_h)_{xx})}{\partial t}, v_h\right)_h + \left(\frac{2}{3} \frac{\partial I_N f(u_h)}{\partial x}, 4v_h - (v_h)_{xx}\right) + \left(\frac{1}{3} I_N(u_h(u_h)_x), 4v_h - (v_h)_{xx}\right)_h = 0.$$

Substituting the equality  $4v_h - (v_h)_{xx} = u_h$ , we have

$$\left(\frac{\partial(u_h - (u_h)_{xx})}{\partial t}, v_h\right)_h + \left(\frac{2}{3} \frac{\partial I_N f(u_h)}{\partial x}, u_h\right) + \left(\frac{1}{3} I_N(u_h(u_h)_x), u_h\right)_h = 0.$$

Notice that

$$\begin{aligned} \left(\frac{2}{3} \frac{\partial I_N f(u_h)}{\partial x}, u_h\right) &= -\left(\frac{2}{3} I_N f(u_h), (u_h)_x\right) \\ &= -\left(\frac{2}{3} I_N f(u_h), (u_h)_x\right)_h, \end{aligned}$$

and

$$\begin{aligned} \left(\frac{\partial(u_h - (u_h)_{xx})}{\partial t}, v_h\right)_h &= \left(\frac{\partial(u_h - (u_h)_{xx})}{\partial t}, v_h\right) \\ &= \left(\frac{\partial u_h}{\partial t}, v_h - (v_h)_{xx}\right) \\ &= \left(\frac{\partial u_h}{\partial t}, v_h - (v_h)_{xx}\right)_h \end{aligned}$$

due to the exactness of the quadrature rule, so we get

$$\left(\frac{\partial u_h}{\partial t}, v_h - (v_h)_{xx}\right)_h - \left(\frac{2}{3} I_N f(u_h), (u_h)_x\right)_h + \left(\frac{1}{3} I_N(u_h(u_h)_x), u_h\right)_h = 0.$$

And by the definition of the discrete  $L^2$  norm and  $f(u) = \frac{u^2}{2}$ , it implies

$$\left(\frac{\partial u_h}{\partial t}, v_h - (v_h)_{xx}\right)_h = 0.$$

Recalling the Lemma 2.1, it leads to the stability results of  $v_h$ . □

Similarly,  $L^2$  norm stability theorem for the numerical solution of the collocation scheme III follow directly from the Eq. (13).

**Proposition 2.5** *For the Fourier collocation scheme III, the  $L^2$  norm of  $u_h$  is stable,*

$$\|u_h(\cdot, t)\|_h \leq 2 \|u_h(\cdot, 0)\|_h.$$

In the collocation method the only use of the Fourier approximation is in obtaining the derivative of the numerical approximation in physical space. There are two ways to do the derivative operation. One way uses the Fourier series and possibly a fast Fourier transformation (FFT), while the other employs the direct matrix-vector multiplication. Mathematically they are identical, but computationally different. The computational cost of the matrix-vector product is an  $\mathcal{O}(N^2)$ , rather than the cost of  $\mathcal{O}(N \log(N))$  in the method using expansion coefficients and FFT.

The application of the Fourier collocation method is easier for nonlinear problems, comparing to the Fourier Galerkin method. This is due to the fact that we can easily evaluate the

nonlinear function  $f(u)$  in terms of points values of  $u$ , while it may be very complicated to express the Fourier coefficients of  $f(u)$  in terms of the expansion coefficients of  $u$ .

Since the DP equation could admit shock solutions even for very smooth initial condition, it is well known that spectral methods will result in the formation of the Gibbs phenomenon. These spurious oscillations will in turn lead to loss of resolution and render the spectral approximations unstable. The existence of entropy solutions is proved in [8], which can be viewed as vanishing viscosity solutions of the DP equation. Similar to the spectral method for the nonlinear conservation laws, this suggest a way to stabilize the spectral method by adding artificial dissipation as

$$u_t + f(u)_x + p_x = \epsilon(-1)^{s+1} \frac{\partial^{2s} u}{\partial x^{2s}}.$$

A direct implementation of this approach may be costly and could introduce additional stiffness which could limit the stable time step. Without extra cost, this can also be done through the use of the exponential spectral filter  $\sigma^e(\eta) = \exp(-\alpha\eta^{2s})$  at each time step, where  $\eta = \frac{k}{N}, k = -N, \dots, N$ .

$$F_N u_h(x, t) = \sum_{k=-N}^N \sigma^e\left(\frac{k}{N}\right) a_k(t) e^{ik\frac{\pi}{L}x}. \tag{17}$$

While the use of filters has a stabilizing effect and improves the global approximation to a discontinuous function, such technique is unable to improve on the quality of the approximation as one approaches the point of discontinuity. Filtering attempts to remove the Gibbs oscillations. In fact, the Gibbs oscillations contain sufficient information to reconstruct an exponentially convergent approximation everywhere provided only that the location of the discontinuity is known.

### 3 Gegenbauer Reconstruction

In the following, we outline the procedure of Gegenbauer reconstruction to recover a piecewise exponentially convergent series to a piecewise analytic function. The spectral projection of the piecewise smooth function yields poor results. Only first order convergence is obtained away from the discontinuities and  $\mathcal{O}(1)$  spurious Gibbs oscillations are exhibited at the discontinuities. In [20], it has been shown that one can reconstruct a rapidly converging Gegenbauer expansion based on the first  $2N + 1$  Fourier coefficients of a function  $f(x)$ . The point values of  $f(x)$  can be recovered with exponential accurate in the maximum norm up to the discontinuity or the boundary. This methodology has also been extended to handle the piecewise analytic functions with singularities in [7]. Here we use the Gegenbauer post-processing method to eliminate the Gibbs phenomenon and recover the piecewise smooth functions with spectral accuracy.

The Gegenbauer polynomials  $C_k^\lambda(x)$ , for  $\lambda \geq 0$ , are orthogonal with respect to the weight function  $(1-x^2)^{\lambda-\frac{1}{2}}$  over the interval  $[-1, 1]$ . They can be expressed by Rodrigues’s formula, or conveniently computed by the following recurrence formula

$$kC_k^\lambda(x) = 2(k + \lambda - 1)x C_{k-1}^\lambda(x) - (k + 2\lambda - 2)C_{k-2}^\lambda(x).$$

The maximum of the Gegenbauer polynomial is achieved at the boundary

$$|C_k^\lambda(x)| \leq C_k^\lambda(1), \quad -1 \leq x \leq 1,$$

and  $C_k^\lambda(1) = \frac{\Gamma(2\lambda+n)}{n!\Gamma(2\lambda)}$ . The Gegenbauer polynomial series of the function  $f(x)$  is defined by

$$f(x) = \sum_{k=0}^{\infty} \tilde{f}_k^\lambda C_k^\lambda(x),$$

where the Gegenbauer coefficient is defined by

$$\tilde{f}_k^\lambda = \frac{1}{h_k^\lambda} \int_{-1}^1 (1-x^2)^{\lambda-\frac{1}{2}} C_k^\lambda(x) f(x) dx,$$

with the normalized constant

$$h_k^\lambda = \sqrt{\pi} C_k^\lambda(1) \frac{\Gamma(\lambda + \frac{1}{2})}{(\lambda + k)\Gamma(\lambda)}.$$

The first  $M + 1$  terms of the Gegenbauer expansion

$$f_M(x) = \sum_{k=0}^M \tilde{f}_k^\lambda C_k^\lambda(x),$$

converges exponentially to an analytic function  $f(x)$  in  $[-1, 1]$ .

From the first  $2N + 1$  Fourier coefficients of the piecewise smooth function, the Gegenbauer post-processing method can recover the exponential accuracy by the Gegenbauer expansion in the smooth region of the function, provided that the  $M$  and  $\lambda$  in the expansion is proportional to the number of the Fourier mode  $N$ . To perform the Gegenbauer post-processing method, it is critical to identify the smooth region of function from its finite Fourier partial expansion. We will use the approach developed in [16–18] to detect the discontinuity or the edge of the piecewise smooth function from its Fourier partial sum, which is based on the fact that the conjugate Fourier partial sum  $S_N[f] = \sum_{k=1}^N (a_k \sin kx - b_k \cos kx)$  approaches the singular support of the function as  $N$  approaches infinity. However, the convergence rate of the conjugate Fourier partial sum is so slow at the rate  $\mathcal{O}(1/\log N)$ . To accelerate the convergence rate, the generalized conjugate partial sum  $\tilde{S}_N[f] = \sum_{k=1}^N \sigma(\frac{k}{N})(a_k \sin kx - b_k \cos kx)$  is formed, where  $\sigma(k/N)$  is the concentration factor. If the concentration factor  $\sigma(\cdot)$  is a non-decreasing  $C^2$  function satisfying  $\int_{1/N}^1 \frac{\sigma(x)}{x} dx \xrightarrow{N \rightarrow \infty} -\pi$  with  $N$  approaches infinity, then  $\tilde{S}_N[f]$  converges to the jump of the function  $f(x)$  with the rate  $|\tilde{S}_N[f](x)| \leq Const(\frac{\log N}{N} + |\sigma(\frac{1}{N})|)$  when  $x$  is away from the discontinuities. When the admissible polynomial concentration factor  $\sigma^p(x) = -\pi p x^p$  is employed, the generalized conjugate Fourier partial sum is equivalent to the differential Fourier partial sum for odd  $p = 2q + 1$

$$\tilde{S}_N[f] = \sum_{k=1}^N \sigma^p(\frac{k}{N})(a_k \sin kx - b_k \cos kx) = (-1)^q \frac{\pi p}{N^p} \frac{d^p}{dx^p} f_N(x).$$

By amplifying the scales  $T = N^{r/2}(\tilde{S}_N[f])^r$ , the enhanced generalized Fourier partial sum was developed in [18] to detect the discontinuities as

$$\tilde{S}_N^e[f] = \begin{cases} \tilde{S}_N[f], & T > J_{crit} \\ 0 & T < J_{crit}. \end{cases}$$

**Table 1** Accuracy test for smooth soliton solutions in Example 4.1:  $L^2$  and  $L^\infty$  errors of  $u$ , at time  $t = 1$  in the domain  $[-75, 75]$

| N                        | 36       | 48       | 60      | 72      | 84      | 96      | 108     |
|--------------------------|----------|----------|---------|---------|---------|---------|---------|
| $\ u - u_h\ _{L^2}$      | 7.42E-04 | 1.12E-04 | 1.28E-5 | 2.19E-6 | 3.81E-7 | 5.48E-8 | 9.55E-9 |
| $\ u - u_h\ _{L^\infty}$ | 3.11E-03 | 5.69E-04 | 3.20E-5 | 9.92E-6 | 1.59E-6 | 2.68E-7 | 3.81E-8 |

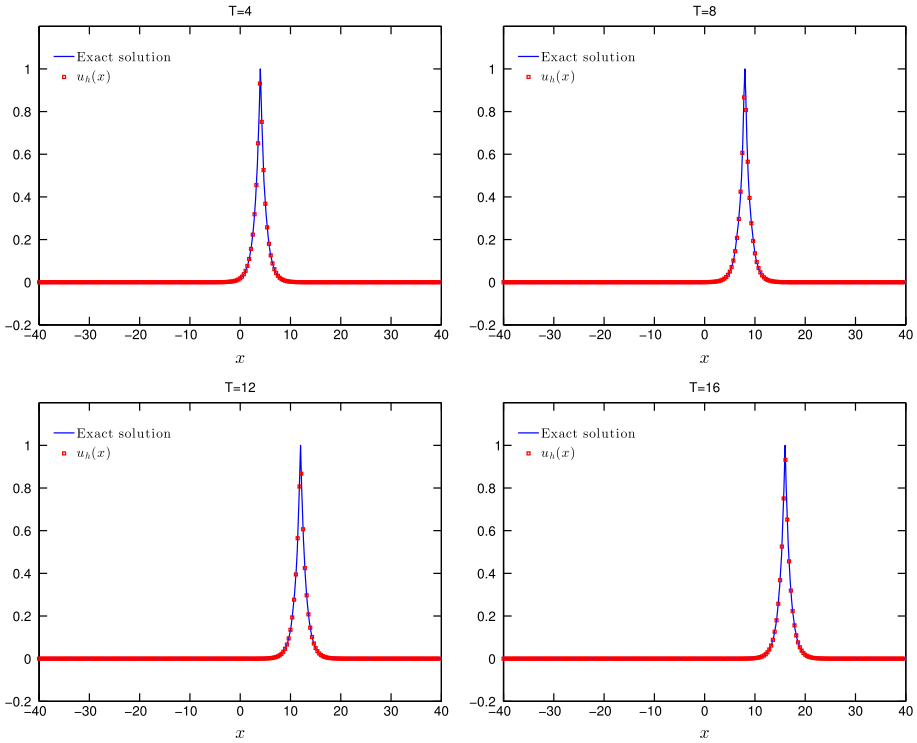


**Fig. 1** Numerical results of the peakon solitons at different times  $t = 4, 8, 12$  and  $16$  with  $N = 256$  in the domain  $[-40, 40]$ , comparing with the exact solution

Noticing that  $\sigma^r(1/N) \sim (N^{-r})$ ,  $T$  converges to the discontinuities at the rate  $\mathcal{O}(N^{r/2}([f])^r)$  and  $\mathcal{O}(N^{-r/2})$  in the smooth region, which separates the scales significantly. And  $J_{crit}$  is an  $\mathcal{O}(1)$  threshold parameter for the jump discontinuities. The discontinuity detection method is crucial for us to pinpoint the discontinuity and perform the Gegenbauer post-processing method in the smooth region.

### 4 Numerical Examples

With the post-processing method from the last section, we will implement the Fourier spectral methods that yields high accuracy to the DP equation and resolves the shock discontinuity. The steps of the full Fourier spectral method are:

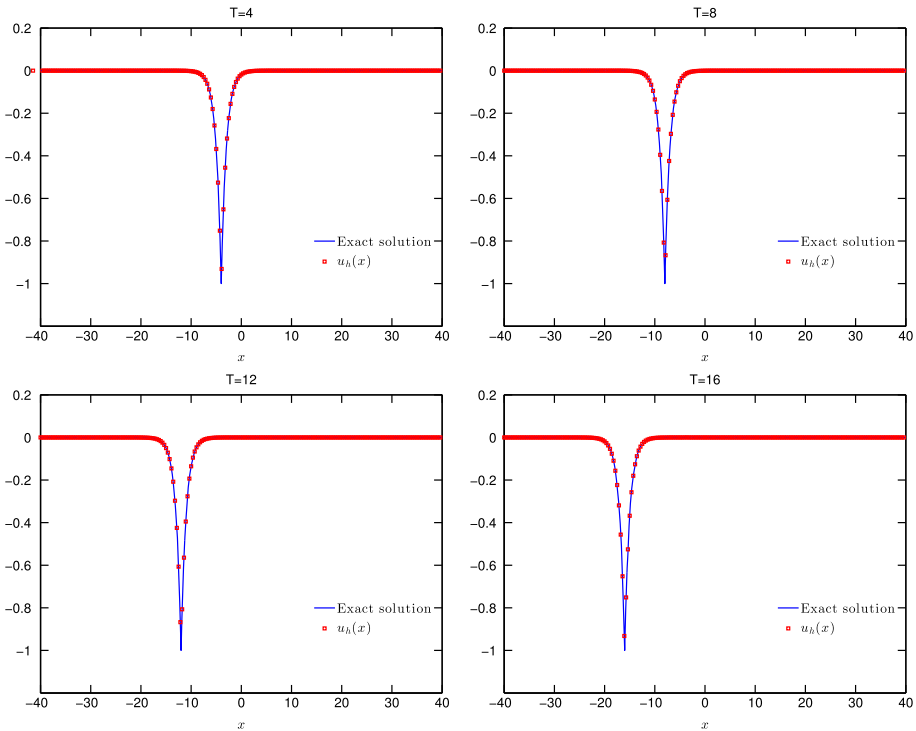


**Fig. 2** Numerical results of the anti-peakon solitons at different times  $t = 4, 8, 12$  and  $16$  with  $N = 256$  in the domain  $[-40, 40]$ , comparing with the exact solution

- Compute the approximation of  $u_h(x, T)$  by the Fourier spectral scheme I, II or III, coupled with the explicit TVD Runge-Kutta time discretization.
- Locate the shock discontinuities and determine the smooth intervals by employing the discontinuity detect method.
- If there are discontinuities, perform the Gegebauer reconstruction to obtain  $(u_h)_M(x, T)$  in each identified smooth interval.

We emphasize that only the first step, the Fourier spectral approximation, is time-implemented. And subsequent steps are only performed once, at the final time  $T$ .

In this section we provide numerical examples to illustrate the accuracy and capability of the proposed algorithm. For the time discretization method, we adopt the explicit TVD Runge-Kutta method [31], due to the total variation bounded property of the DP equation. Even with the third order spatial derivative, the time step for both schemes is  $\Delta t \approx 1/N$ , because the inverse operator of  $I - \partial_{xx}$  is applied at each time step. In the following simulations, the Fourier Galerkin and collocation schemes perform very similarly. So we only show the numerical results from the Fourier collocation scheme for simplicity. For the problems without the analytic solutions, the numerical results are shown to be numerically convergent, with the aid of successive mesh refinement. These numerical simulation mainly comes from the paper of Xu and Shu [33] for easily comparison. When the discontinuity occurs in the test, we need the exponential filter to stabilize the scheme, but small enough not to ruin the accuracy of the scheme. We choose the parameters in the filter as  $s = 16$  and  $\alpha = -\log \epsilon_M$ , with  $\epsilon_M$  represents the machine accuracy. The effect of the filter is thus similar to add a small

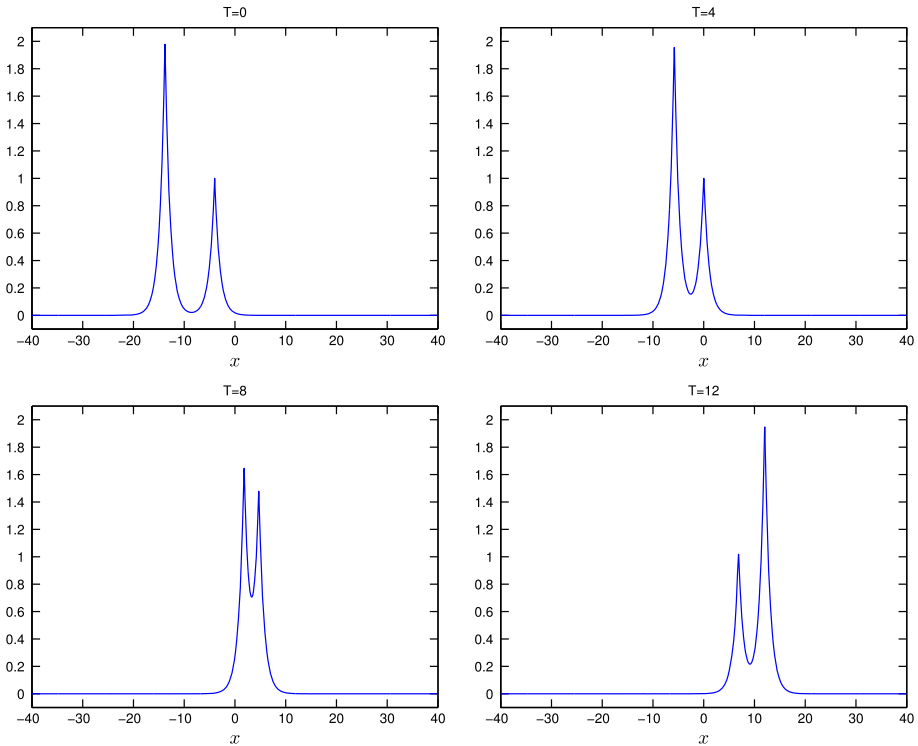


**Fig. 3** Numerical results of two-peakon interaction at different times  $t = 4, 8, 12$  and  $16$  with  $N = 256$  in the domain  $[-40, 40]$

dissipative term with  $\epsilon = \frac{\alpha}{\Delta t N^{2s}}$ . Based on Theorem 4.1 in the paper [20], the parameters  $\lambda = \alpha N$  and  $M = \beta N$  in the unit domain for the Gegenbauer reconstruction are chosen by setting  $\alpha = \beta = \frac{1}{16}$  which is less than the bound  $\frac{2}{27}$  in the case of  $N = 256$ . We also choose the computational domain large enough, such that the solution at the boundary is small enough for the periodic boundary condition holds approximately at the truncation error level. All these numerical results can be obtained efficiently in seconds owe to FFT.

*Example 4.1* Accuracy test for smooth soliton solutions

Consider the traveling wave solution  $u(x, t) = U(x - ct)$  of the DP equation, where  $c$  is the wave speed. Let  $\xi = x - ct$ , and assume  $\lim_{\xi \rightarrow \infty} U(\xi) = A$ . The smooth soliton solutions have been constructed explicitly in [35]. When we set  $A = 1$  and  $c = 5$ , an explicit formula of the smooth soliton solution can be obtained as

$$U(\xi) = A \left( (4 - \sqrt{5}) - \frac{2\sqrt{5}}{X(\xi)^2 - 1} \right),$$

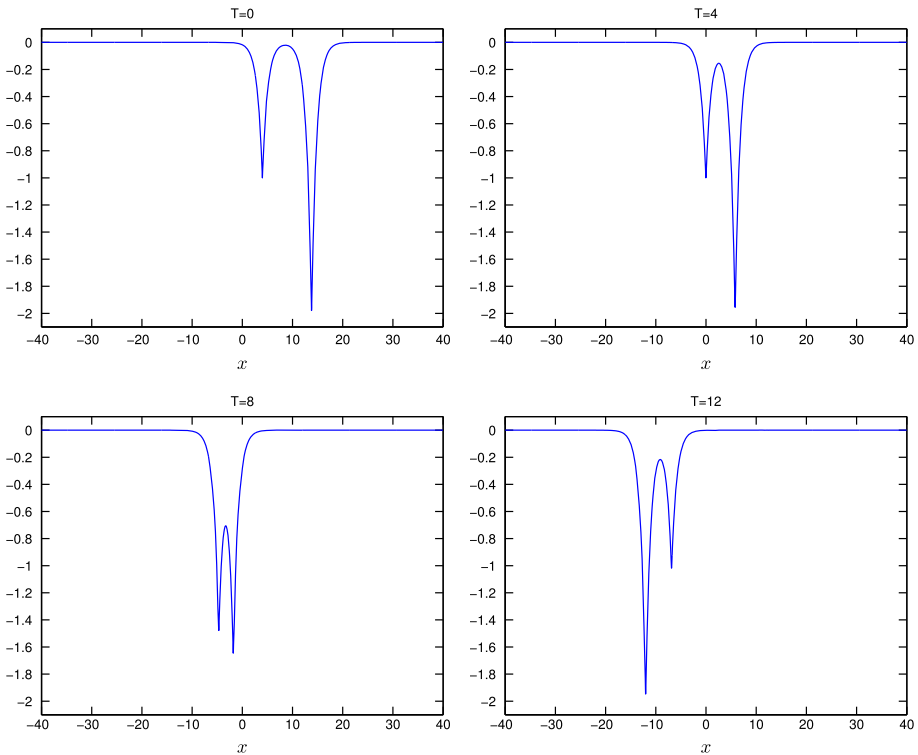


**Fig. 4** Numerical results of anti-two-peakon interaction at different times  $t = 4, 8, 12$  and  $16$  with  $N = 256$  in the domain  $[-40, 40]$

where  $X(\xi)$  is defined by

$$\begin{aligned}
 X(\xi) = & \left( -\frac{7+3\sqrt{5}}{3}b + \frac{38+17\sqrt{5}}{27}b^3 + \sqrt{\frac{2+\sqrt{5}}{27} + \frac{517+231\sqrt{5}}{54}b^2 - \frac{521+233\sqrt{5}}{54}b^4} \right)^{\frac{1}{3}} \\
 & + \left( -\frac{7+3\sqrt{5}}{3}b + \frac{38+17\sqrt{5}}{27}b^3 - \sqrt{\frac{2+\sqrt{5}}{27} + \frac{517+231\sqrt{5}}{54}b^2 - \frac{521+233\sqrt{5}}{54}b^4} \right)^{\frac{1}{3}} \\
 & + \frac{2+\sqrt{5}}{3}b,
 \end{aligned}$$

with  $b = \frac{1+e^{|\xi|}}{1-e^{|\xi|}}$ . The  $L^2$  and  $L^\infty$  errors and the numerical orders of accuracy for the numerical solution  $u_h$  at time  $t = 1$  in the domain  $[-75, 75]$  are contained in Table 1. The numerical solution  $u_h$  is obtained by the Fourier collocation scheme with the exponential filter, even the filter is not necessary for this test. We also set the time step small enough so that the spatial discretization error is dominated in the simulation. From the table, it shows that the method can achieve the spectral accuracy. As we expected, the filter does not ruin the accuracy.

*Example 4.2* Single peakon and anti-peakon traveling solutions

In this example, we present the traveling waves of peakon and anti-peakon solutions  $u(x, t) = ce^{-|x-ct|}$ , and  $u(x, t) = -ce^{-|x+ct|}$ . The peakon and anti-peakon solutions do not have enough regularity, so the DP equation is satisfied in the distribution sense. We choose the traveling speed  $c = 1$  and the computational domain  $[-40, 40]$  with  $N = 256$ . In Figs. 1 and 2, the peakon and anti-peakon profiles are shown at times  $t = 4, 8, 12$  and  $16$  with the exact solutions. These traveling waves are smooth everywhere except the wave crest. We can see that the moving peakon and anti-peakon are well resolved without any numerical oscillation.

*Example 4.3* Two-peakons interaction and two-anti-peakons interaction:

In this example, we consider the two-peakons interaction of the DP equation with the initial condition

$$u = c_1e^{-|x-x_1|} + c_2e^{-|x-x_2|},$$

where the parameters  $c_1 = 2, c_2 = 1, x_1 = -13.792$  and  $x_2 = -4$ . The same parameters are used in the two-anti-peakons interaction, with the initial condition

$$u = -c_1e^{-|x+x_1|} - c_2e^{-|x+x_2|}.$$

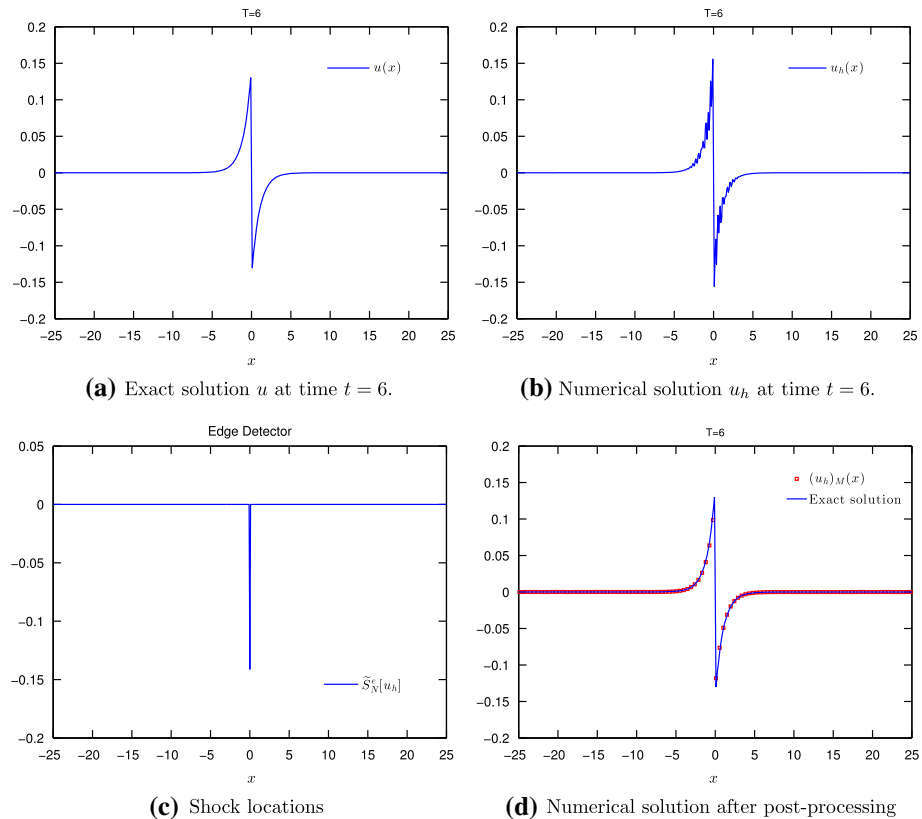


**Fig. 5** Numerical results of shock peakon solution at time  $T = 6$  with  $N = 256$  in the domain  $[-25, 25]$ , before and after the Gegenbauer post-processing, comparing with the exact solution

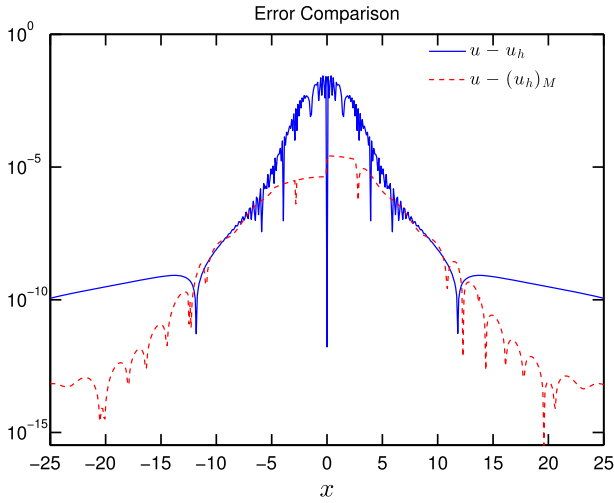


**Fig. 6** The comparison of the errors before and after the Gegenbauer post-processing, in the Example 4.4

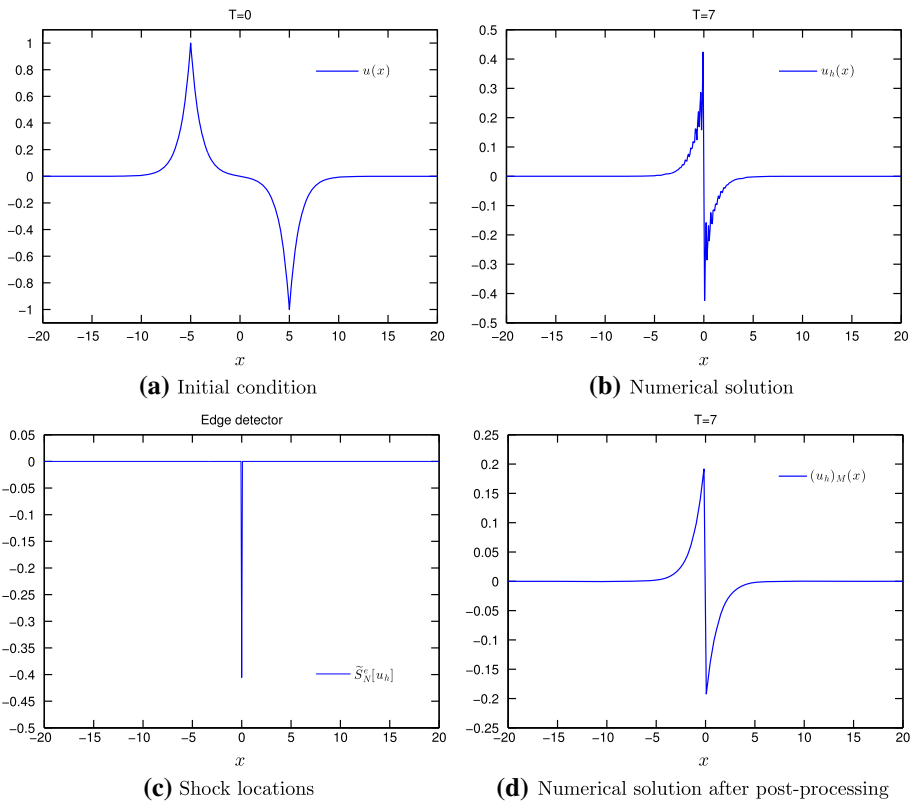


**Fig. 7** Numerical results of shock peakon solution at time  $T = 7$  with  $N = 256$  in the domain  $[-20, 20]$ , before and after the Gegenbauer post-processing

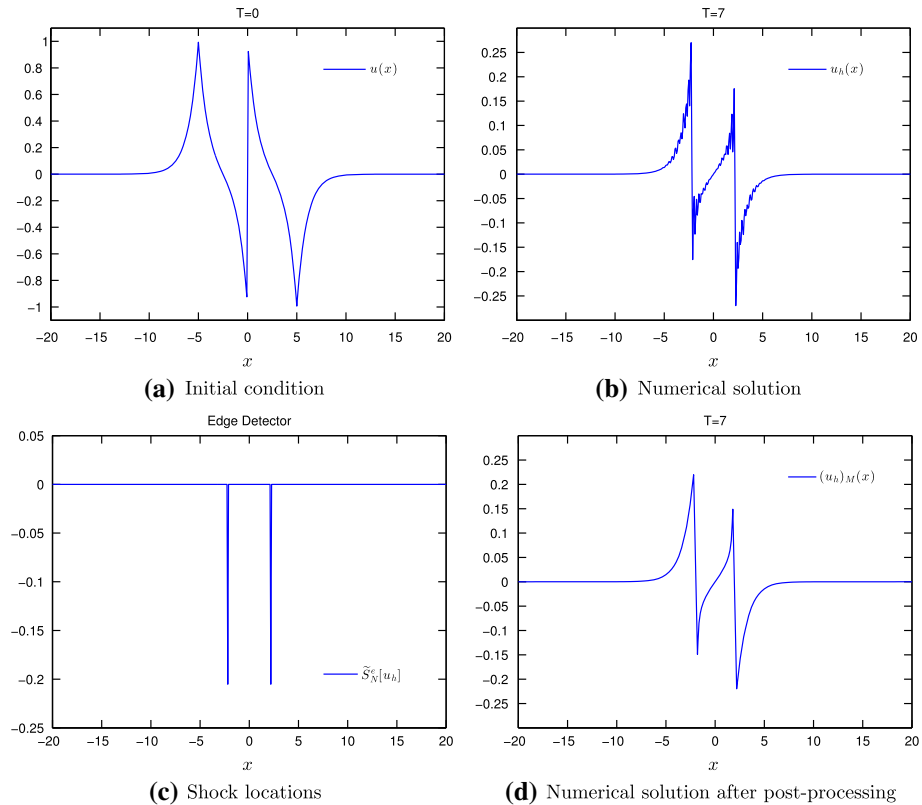


**Fig. 8** Numerical results of the interaction among peakon, anti-peakon and one stationary shock peakon, at time  $t = 7$  with  $N = 256$  in the domain  $[-20, 20]$

In these interactions, the soliton should preserve its shape and velocity before and after encountering a nonlinear interaction with other similar soliton. In Figs. 3 and 4, the interactions profiles show at times  $t = 0, 4, 8$  and  $12$  in the domain  $[-40, 40]$  with  $N = 256$ . We can see that the moving peakons interactions are resolved very well. And numerically it shows that these interactions are elastic processes.

*Example 4.4* Shock peakon solution

The DP equation also admits shock peakon solution

$$u(x, t) = -\frac{1}{t + 1} \text{sign}(x)e^{-|x|},$$

which contains a discontinuity at  $x = 0$ . The presence of shock peakon solutions means that the DP equation admits solution that is less regular than the CH equation, which makes the difference between the DP and CH equations. In this example, the simulation is performed in the domain  $[-25, 25]$  with  $N = 256$ . Because of the shock discontinuity in the solution, the Gegenbauer reconstruction is used at the final time step to remove the numerical oscillations. In the Fig. 5, the numerical results  $u_h$  and post-processed  $(u_h)_M$  have been showed comparing with the exact solution. We can see that there are some spurious oscillations near the discontinuity of the numerical solution  $u_h$  due to the Gibbs phenomenon. But after the

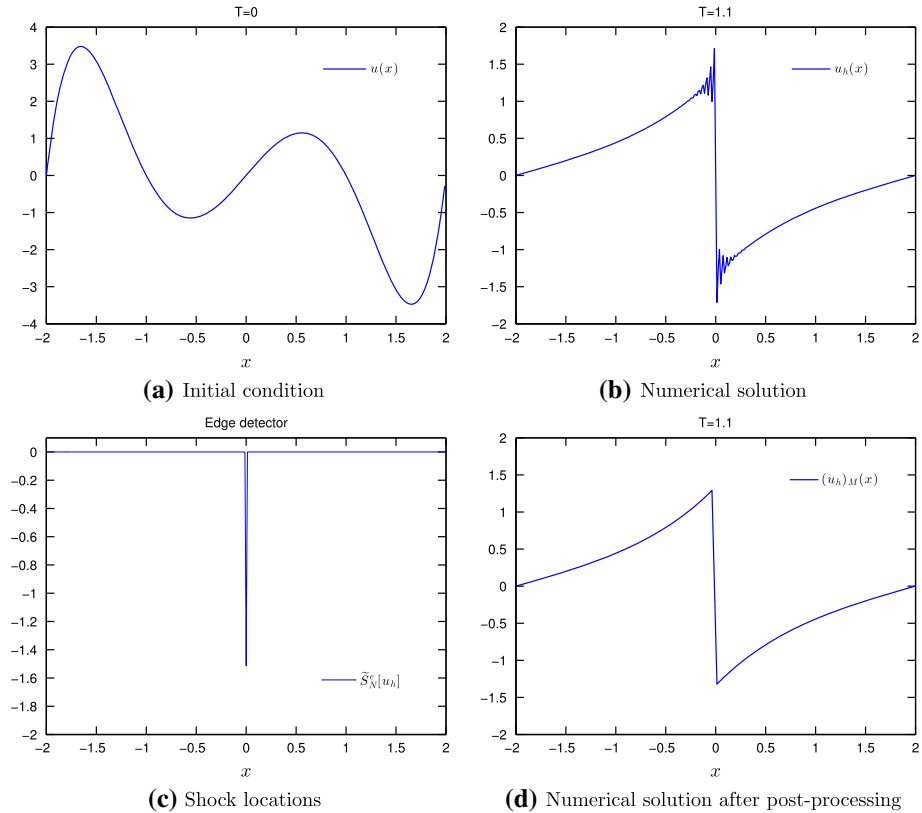


**Fig. 9** Numerical results of shock formation at time  $t = 1.1$  with  $N = 256$ , in the domain  $[-2, 2]$

Gegenbauer post-processing, the solution can be resolved very well by the post-processed solution  $(u_h)_M$  as we expected. Also, Fig. 6 shows the numerical errors before and after the post-processing. We find that the post-processing step reduces the error and recovers the accuracy near the discontinuity digitally.

*Example 4.5* Peakon and anti-peakon interaction

For the DP equation, the shock can also be formed between the peakon and anti-peakon interaction, with the initial condition

$$u(x, 0) = c_1 e^{-|x-x_1|} - c_2 e^{-|x-x_2|};$$

where  $c_1 = 1, c_2 = 1, x_1 = -5$  and  $x_2 = 5$ . In the CH equation, the peakon and anti-peakon will pass through each other after the collision. But the DP equation will generate shocks in the collision. Figure 7 shows the numerical solution  $u_h$  and the post-processed solution  $(u_h)_M$  with  $0.31 N = 256$  in the domain  $[-20, 20]$ . Similarly, the shock causes artificial oscillations in the numerical result  $u_h$ . With the help of Gegenbauer post-processing, these oscillation can be eliminated and the shock is fully resolved in the numerical result  $(u_h)_M$ .

#### Example 4.6 Triple interaction

In this example, we consider the interaction among peakon, anti-peakon and one stationary shock peakon of the DP equation, with the initial condition

$$u(x, 0) = e^{-|x+5|} + \text{sign}(x)e^{-|x|} - e^{-|x-5|}.$$

The computational domain is  $[-20, 20]$ . Figure 8 shows the numerical results at time  $t = 7$  with  $N = 256$ . From the figure, it shows that there are two shocks formed at this time. Using the shock detector method described in the last section, we can identify the shock locations clearly. Then, the Gegebauer reconstruction method is adopted to eliminated the artificial oscillation in the numerical solution  $u_h$  caused by the shocks efficiently. Then the solution with multiple shocks are resolved very well by the numerical solution  $(u_h)_M$ .

#### Example 4.7 Shock formation

In this example, we consider the shock formation with the smooth initial condition:

$$u(x, 0) = e^{0.5x^2} \sin(\pi x).$$

Figure 9 shows the numerical results  $u_h$  and  $(u_h)_M$  at time  $t = 1.1$  with  $N = 256$  in the domain  $[-2, 2]$ . To remove the spurious oscillation in the numerical solution  $u_h$ , Gegenbauer post-processing is applied to  $u_h$  and then the sharp shock detecting numerical result  $(u_h)_M$  is obtained. We can see that even with the smooth initial condition shock appears in finite time. These numerical tests show that the Fourier spectral methods coupled with the Gegenbauer reconstruction can resolve the solution of the DP equation very well, with or without the discontinuity.

## 5 Conclusion

We developed the Fourier Galerkin and collocation spectral methods for the DP equation.  $L^2$  stability is proved for both methods. The DP equation are prone to develop discontinuous solutions in finite time even with smooth initial condition. To deal with the Gibbs phenomenon for the discontinuous solution, Gegenbauer reconstruction is adopted to resolve the shock successfully. Numerical examples are given to show the accuracy and the capacity of these methods. These methods are also very efficient, especially for the collocation method. This approach has been applied to some other PDE admitting the discontinuous solution [17], after the stable Fourier spectral method has been developed. Also, the Chebyshev collocation can also be applied to the DP equation with different kind of boundary conditions in future.

## References

1. Bernardi, C., Maday, Y.: Spectral methods. In: Ciarlet, P.G., Lions, J.L. (eds.) Handbook of Numerical Analysis. Techniques of scientific computing, vol. 5, pp. 209–486. Elsevier, Amsterdam (1997)
2. Boyd, J.P.: Chebyshev and Fourier Spectral Methods, 2nd edn. Dover Publication, New York (2001)
3. Camassa, R., Holm, D.D.: An integrable shallow water equation with peaked solitons. Phys. Rev. Lett. **71**, 1661–1664 (1993)
4. Canuto, C., Hussaini, M.Y., Quarteroni, A., Zang, T.A.: Spectral Methods in Fluid Dynamics. Springer, Berlin (1988)
5. Canuto, C., Hussaini, M.Y., Quarteroni, A., Zang, T.A.: Spectral Methods: Fundamentals in Single Domains. Springer, Berlin (2006)

6. Canuto, C., Hussaini, M.Y., Quarteroni, A., Zang, T.A.: *Spectral Methods: Evolution to Complex Geometries and Applications to Fluid Dynamics*. Springer, Berlin (2007)
7. Chen, Z., Shu, C.-W.: Recovering exponential accuracy from collocation point values of smooth functions with end-point singularities conservative schemes. *J. Comput. Phys.* (appear)
8. Coclite, G.M., Karlsen, K.H.: On the well-posedness of the Degasperis–Procesi equation. *J. Funct. Anal.* **233**, 60–91 (2006)
9. Coclite, G.M., Karlsen, K.H.: On the uniqueness of discontinuous solutions to the Degasperis–Procesi equation. *J. Differ. Equ.* **234**, 142–160 (2007)
10. Coclite, G.M., Karlsen, K.H., Risebro, N.H.: Numerical schemes for computing discontinuous solutions of the Degasperis–Procesi equation. *IMA J. Numer. Anal.* **28**(1), 80–105 (2008)
11. Constantin, A., Lannes, D.: The hydrodynamical relevance of the Camassa–Holm and Degasperis–Procesi equations. *Arch. Rat. Mech. Anal.* **192**, 165–186 (2009)
12. Degasperis, A., Procesi, M.: Asymptotic integrability. In: Degasperis, A., Gaeta, G. (eds.) *Symmetry and Perturbation Theory*, pp. 23–37. World Scientific Publishers, River Edge, NJ (1999)
13. Degasperis, A., Holm, D.D., Hone, A.: A new integrable equation with peakon solutions. *Theor. Math. Phys.* **133**, 1463–1474 (2002)
14. Dullin, H.R., Gottwald, G.A., Holm, D.D.: On asymptotically equivalent shallow water wave equations. *Phys. D* **190**, 1–14 (2004)
15. Feng, B., Liu, Y.: An operator splitting method for the Degasperis–Procesi equation. *J. Comput. Phys.* **228**, 7805–7820 (2009)
16. Gelb, A., Tadmor, E.: Detection of edges in spectral data II. nonlinear enhancement. *Appl. Comput. Harmon. Anal.* **7**, 101–135 (1999)
17. Gelb, A., Tadmor, E.: Enhanced spectral viscosity approximations for conservation laws. *Appl. Numer. Math.* **33**, 3–21 (2000)
18. Gelb, A., Tadmor, E.: Detection of edges in spectral data II. nonlinear enhancement. *SIAM J. Numer. Anal.* **38**, 1389–1408 (2000)
19. Gottlieb, D., Orszag, S.A.: *Numerical Analysis of Spectral Methods: Theory and Applications*. SIAM-CBMS, Philadelphia (1977)
20. Gottlieb, D., Shu, C.-W.: On the Gibbs phenomenon and its resolution. *SIAM Rev.* **39**, 644–668 (1998)
21. Guo, B.-Y.: *Spectral Methods and Their Applications*. World Scientific, Singapore (1998)
22. Hesthaven, J.S., Gottlieb, S., Gottlieb, D.: *Spectral Methods for Time-Dependent Problems*. Cambridge Monographs on Applied and Computational Mathematics. Cambridge University Press, Cambridge (2007)
23. Hoel, H.: A numerical scheme using multi-shockpeakons to compute solutions of the Degasperis–Procesi equation. *Electron. J. Differ. Equ.* **2007**, 1–22 (2007)
24. Ivanov, R.: Water waves and integrability. *Philos. Trans. R. Soc. A* **365**, 2267–2280 (2007)
25. Johnson, R.S.: The classical problem of water waves: a reservoir of integrable and nearly-integrable equations. *J. Nonlinear Math. Phys.* **10**(Supplement 1), 72–92 (2003)
26. Karniadakis, G.E., Sherwin, S.T.: *Spectral/hp Element Methods for CFD*. Oxford University Press, Oxford (1999)
27. Liu, H., Huang, Y., Yi, N.: A Conservative discontinuous Galerkin Method for the Degasperis–Procesi Equation, *Methods Appl. Anal.* (submitted)
28. Lundmark, H.: Formation and dynamics of shock waves in the Degasperis–Procesi equation. *J. Nonlinear Sci.* **17**, 169–198 (2007)
29. Miyatake, Y., Matsuo, T.: Conservative finite difference schemes for the Degasperis–Procesi equation. *J. Comput. Appl. Math.* **236**, 3728–3740 (2012)
30. Shen, J., Tang, T., Wang, L.L.: *Spectral Methods: Algorithms, Analysis and Applications*. Springer, Berlin (2011)
31. Shu, C.-W., Osher, S.: Efficient implementation of essentially non-oscillatory shockcapturing schemes. *J. Comput. Phys.* **77**, 439–471 (1988)
32. Xu, Y., Shu, C.W.: A local discontinuous Galerkin method for the Camassa–Holm equation. *SIAM J. Numer. Anal.* **46**, 1998–2021 (2008)
33. Xu, Y., Shu, C.W.: Local discontinuous Galerkin methods for the Degasperis–Procesi equation. *Commun. Comput. Phys.* **10**, 474–508 (2011)
34. Yu, C.H., Sheu, T.W.H.: A dispersively accurate compact finite difference method for the Degasperis–Procesi equation. *J. Comput. Phys.* **236**, 493–512 (2013)
35. Zhang, G., Qiao, Z.: Cuspons and smooth solitons of the Degasperis–Procesi equation under inhomogeneous boundary condition. *Math. Phys. Anal. Geom.* **10**, 205–225 (2007)